AJP

ISSN : 0971 - 3093

Vol 28, Nos 10-12, October-December 2019

ASIAN JOURNAL OF PHYSICS

An International Peer Reviewed Research Journal

Advisory Editors : W. Kiefer & FTS Yu

A Special Issue

Dedicated to

Prof Kehar Singh

Formerly Professor of Physics

at IIT Delhi

Guest Editor : R. S. Sirohi

ap

ANITA PUBLICATIONS

FF-43, 1st Floor, Mangal Bazar, Laxmi Nagar, Delhi-110 092, India

B O : 2, Pasha Court, Williamsville, New York-14221-1776, USA

Asian Journal of Physics

(A Non-Profitable Publication)

ap

Asian Journal of Physics
Vol. 28, Nos 10-12 (2019) 1091-1102
Available on: www.asianjournalofphysics.in

Multi-pass, multi-beam and multi-wavelength optical interferometries

Rajpal S Sirohi
Department of Physics
Alabama A&M University, Huntsville, AL 35802, USA

This article is dedicated to Prof Kehar Singh for his significant contributions to Optics and Photonics

Optical interferometry is perhaps the oldest precision measurement technique that has evolved in its various variants due to the developments in optical sources and detector systems, and varied applications. Some of the variants are developed to enhance the accuracy of measurement and also the ease of measurement. This paper discusses the theory of multi-pass, multi-beam and multi-wavelength interferometries.

Keywords: Two-beam Interferometry, Multi-beam Interferometry, Multi-wavelength Interferometry

1 Introduction

Interferometry is a technique of precise measurement that is based on wave-phenomenon: two or more waves are superposed. When light waves are superposed, it is called optical interferometry. Interferometry measures the phase difference and hence the measuring stick is the wavelength. Many diverse processes can alter the phase of light wave and hence large number of parameters can be indirectly measured. These include refractive index, temperature, pressure, concentration, angle, magnetic field, electric field and host of other parameters. Of course it measures length and changes in length. It has, therefore, been used in many disciplines of science, engineering, technology, medicine etc. It is an essential technique in an optical production facility and the quality of optical instruments is the testimony of its strength as a measurement technique. There are plenty of books that describe interferometry and its applications [1-4].

2 Theory

To keep the material simple and understandable, it is assumed that the source of light delivers a monochromatic and coherent wave. Further light being an electromagnetic wave, its polarization state is ignored. A wave, propagating in positive z-direction, is then expressed as

$$a(x, y, z:t) = a_0 \, e^{i(\omega t - kz + \varepsilon)}$$

where a_0 is the amplitude, being constant for a plane wave; ω is the angular frequency, k is the propagation parameter and ε is the initial phase of the wave. To observe interference phenomenon, two or more waves are superposed. In two-beam interferometry, one wave is the object wave, which has acquired information about the variable to be measured and other one is a reference wave. These two waves are spatially coherent and hence are derived from the same parent wave.

Figure 1 shows a schematic of a two-beam interferometer: one beam interacts with the object whose parameters are to be measured and its phase gets modulated while the other beam acts as a reference. A combiner superposes these two beams to interfere. Superposition of two waves results in a wave described by

$$a(x,y,z;t) = a_{01} \, e^{i(\omega t - kz + \varepsilon_1)} + a_{02} \, e^{i(\omega t - kz + \varepsilon_2)}$$

Corresponding author :
e-mail: rs_sirohi@yahoo.co.in (Rajpal S Sirohi)

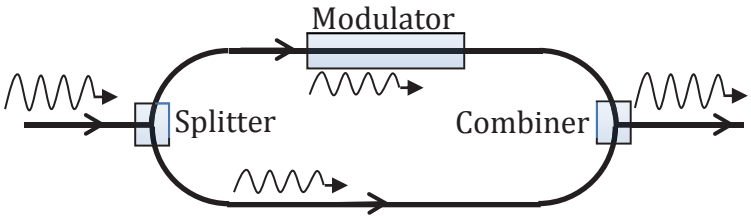

Fig 1. Schematic of a two-beam interferometer

Irradiance in the interference pattern is expressed as

$$I = a(x,y,z;t)\, a^*(x,y,z:t) = I_1 + I_2 + 2\sqrt{I_1 I_2}\cos\delta$$

where, I_1 ($= a_{01}a_{01}^*$) and I_2 ($= a_{02}a_{02}^*$) are the irradiances of individual waves and δ [$= (\varepsilon_1 - \varepsilon_2)$] is the phase difference between them. This irradiance distribution is taken on a plane perpendicular to z-axis. It is seen that the irradiance I depends on δ, being maximum when $\delta = 2m\pi$: m is an integer that takes values 0, ±1, ±2, …. The irradiance is minimum when $\delta = (2m + 1)\pi$. Therefore, at some locations of the screen, the screen will be bright and other locations, it would be dark. In between the irradiance varies cosinusoidally.

However, if the second wave lies in x-z plane, it can be expressed as

$$a_2(x,y,z:t) = a_{02}\, e^{i(\omega t - k_x x - k_z z + \varepsilon_2)}$$

The irradiance distribution in the interference pattern is given by

$$I = I_1 + I_2 + 2\sqrt{I_1 I_2}\cos[k_x x + k_z z - kz + \varepsilon_1 - \varepsilon_2]$$

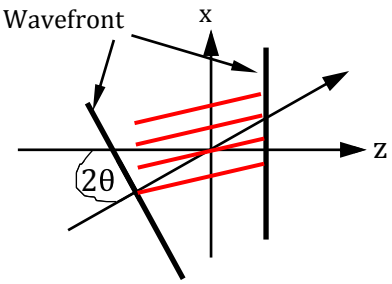

Fig 2. Interference between two waves enclosing an angle 2θ

As shown in the Fig 2, the two plane waves enclose an angle of 2θ. Therefore, $k_x = k \sin 2\theta$ and $k_z = k \cos 2\theta$. Since ($\varepsilon_1 - \varepsilon_2$) is constant, the condition for the bright irradiance is

$$k[x \sin 2\theta + (\cos 2\theta - 1)z] = 2\pi m: m \text{ being an integer}$$

$$x\cos\theta - z\sin\theta = m\lambda/2\sin\theta$$

This equation represents the family of planes, which are separated by $\lambda/2\sin\theta$ in space. When the recording is done on a plane perpendicular to the z-axis, the intersection of these planes with z = constant plane gives straight lines of bright regions interspersed with dark regions: these are called bright and dark fringes. Their separation (spacing) is $\lambda/\sin 2\theta$: this is also called the fringe width. When one of the interfering waves departs from planar form, this departure is manifested as departures in the fringe spacing: fringes no longer remain straight lines. It is this departure, which forms the basis of measurements, as the wavefront is aberrated by the measurand.

Two beam interferometry

Newton's ring experiment is perhaps the first two-beam interferometer, which even today is used to measure the radius of curvature and for testing of flat surface. This was followed by Young's double slit

experiment, which provided the strong support for wave nature of light. Varieties of interferometers were developed in subsequent years for various applications: notable amongst them are Fizeau interferometer, Michelson interferometer, wyman-Green interferometer, Mach-Zehnder interferometer, Rayleigh interferometer, Jamin interferometer. The two-beam interferometers fall under two categories: (i) based on division of wavefront and (ii) based on division of amplitude. Interferometers based on division of wavefront can be truly two-beam. Those based on amplitude division are two-beam interferometers in the restricted sense where either the reflectivity of the surfaces is low so that higher order beams have very small amplitude as compared to first two beams or the coherence of light is adjusted so that higher order beams do not make any contribution to the interference of waves except adding to the background.

Multi-pass Interferometry

Fizeau, Michelson and Twyman Green interferometers are double-pass interferometers and hence the consecutive fringes are separated by λ/2 in path difference. Mach-Zehnder, Jamin and Rayleigh interferometers are single pass interferometers and the fringes are separated by λ in path difference. In order to increase the sensitivity, multi-pass is utilized. In order to amplify imperfections of a mirror, Langenbeck introduced partially coated beam-splitter in front of the mirror of a Twyman-Green interferometer forming a wedge of suitable angle [5]. Multiply reflected beams propagate in different directions. By suitably aligning the reference mirror so that the reference beam interferes with n times reflected beam and suitably filtering this, he demonstrated sensitivity enhancement by a factor of 5. Since the amplitude of multiply reflected beam decreases fast, the amplitude of the reference beam should be suitably adjusted to obtain fringe pattern of good visibility. Fizeau interferometer is also multi-passed for testing the flat surface and moiré phenomenon is used for readout [6]. Bubis described a multi-pass interferometer for testing concave mirror and achieved five-fold increase in sensitivity [7]. An interesting application of multi-pass has been to measure very long radii of concave surfaces in a limited working space using a short measuring slide [8]. Hariharan and Sen presented the theory of fringe formation in double-pass Michelson interferometer and showed that the precision of measurement could be λ/1000 [9].

Multi-pass interferometry requires long coherence length. However, with ingenious design of the interferometer, it can be implemented even with a short-coherence length source. Zhang and Yonemura implemented an improved multi-pass Michelson interferometer for distance measurement by inserting a beam splitter into one arm of the interferometer, resulting in multiple reflections between the end mirror and the beam splitter [10]. This technique uses the fact that the wavelength of a laser diode varies in proportion to the diode's injection current.

Pisani replaced one of the mirrors of a Michelson interferometer with a pair of mirrors enclosing a small angle in which multiple reflections take place and demonstrated picometer sensitivity for displacement measurement [11]. Using similar kind of arrangement for multiple reflections, Joenathan *et al* demonstrated nano-radian angle sensitivity using cyclic interferometer [12,13] and picometer sensitivity in dual-arm multiple-reflection Michelson interferometer [14].

Another method of phase amplification that can be discussed under two-beam interferometry is to record a hologram of the distorted wavefront. Hologram will usually reconstruct the object wave and its higher orders. If the wavefront from the n^{th} order is used in one arm of an interferometer, the interference pattern will exhibit n-fold sensitivity [15].

Multi-beam Interferometry

When large number of waves participates in interference, it falls under multi-beam interferometry. Obvious outcome of this is fringe sharpening. This topic is dealt with under three different sections: (i) superposition of large number of beams of equal amplitude (grating), (ii) superposition of infinite number of beams with geometrically decreasing amplitude (Fabry-Perot) and (iii) finite number of beams with geometrically decreasing amplitude and walk off.

Multiple-beams by wavefront division

A grating consists of N equi-spaced narrow openings, which is illuminated by a collimated beam emanating from a line-source and the diffracted beams, which are of equal amplitudes, are collected by a lens thus making images of the line source in different orders at the focal plane.

A collimated beam of wavelength λ illuminates the grating at an angle ϕ and the diffracted light is collected in the direction θ. The resultant amplitude when N-beams are superposed is given by

$$A = a + ae^{i\delta} + ae^{i2\delta} + \ldots + ae^{i(N-2)\delta} + ae^{i(N-1)\delta} = a\frac{1 - e^{iN\delta}}{1 - e^{i\delta}}$$

where δ is the phase difference between waves from two consecutive grating openings (slits). The phase difference δ is given by

$$\delta = \frac{2\pi}{\lambda} d(\sin\phi + \sin\theta)$$

In practice, the grating is illuminated normally and hence the phase difference δ is given by

$$\delta = \frac{2\pi}{\lambda} d\sin\theta$$

The irradiance distribution at the focal plane of a lens is given by

$$I(\delta) = AA^* = a^2 \frac{1 - e^{iN\delta}}{1 - e^{i\delta}} \frac{1 - e^{-iN\delta}}{1 - e^{-i\delta}} = I_0 \frac{1 - \cos N\delta}{1 - \cos\delta} = I_0 \frac{\sin^2(N\delta/2)}{\sin^2(\delta/2)}$$

The maximum of irradiance distribution occurs when the denominator is zero, i.e., when δ takes values, which are integral multiples of 2π:

$$\delta = \frac{2\pi}{\lambda} d\sin\theta = 2m\pi \longrightarrow\longrightarrow d\sin\theta = m\lambda : m = 0, \pm1, \pm2, \pm3, \ldots \ldots$$

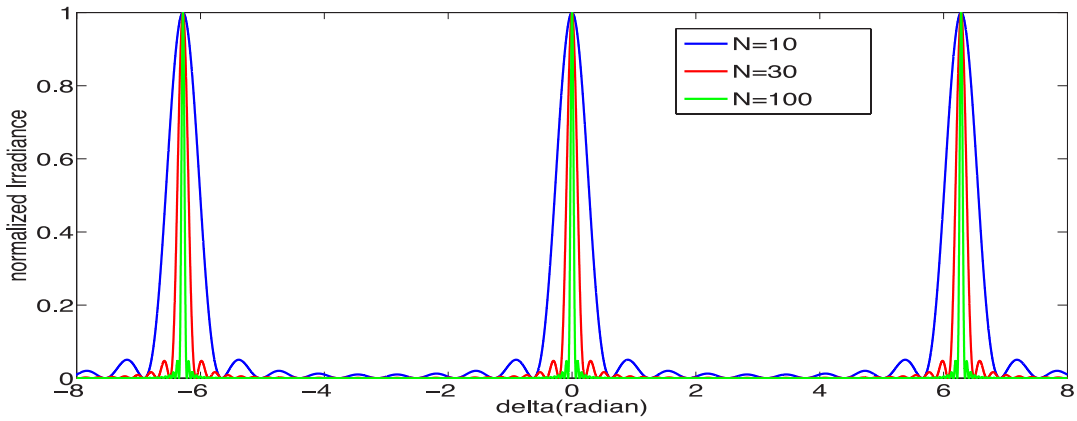

Fig 3. Irradiance distribution in an interference pattern with finite number of beams of equal amplitude

The equation $d\sin\theta = m\lambda$ is the grating equation. The grating equation gives the direction in which principal maxima occur. Further the irradiance of principal maxima is $N^2 I_0$. In between the principal maxima there are secondary maxima, which occur wherever the numerator takes a value 1, i.e., $\delta = (2m + 1)\pi/N$. There are thus $(N - 2)$ secondary maxima between two consecutive principal maxima. The irradiance of successive secondary maxima keeps on decreasing due to the value of denominator increasing with increase of δ. The irradiance distribution has been plotted for several values of N in Fig 3: the plot is of normalized irradiance versus phase difference.

According to grating equation, different wavelengths are angularly separated. Using Rayleigh criterion of resolution, the resolving power $\mathcal{R}$ of a grating is given by

$$\mathcal{R} = \frac{\lambda}{\Delta\lambda}$$

where, $\Delta\lambda = \lambda' - \lambda$: λ' and λ are the two wavelengths that are just resolved according to Rayleigh criterion. For a grating, the order m may not exceed three, as the angle of diffraction can at the most be 90°. The free spectral range $\Delta\lambda_{\text{fsr}}$ is the largest wavelength range for a given order that does not overlap the same range in an adjacent order:

$$d\sin\theta = m(\lambda + \Delta\lambda_{\text{fsr}}) = (m+1)\lambda: \qquad \Delta\lambda_{\text{fsr}} = \lambda/m$$

Obviously higher orders have smaller free spectral range.

Multiple beams by amplitude division

A Fabry-Perot interferometer consists of two high reflecting mirrors aligned parallel to each other and whose separation could be varied. A plane parallel plate of thickness t and refractive index n whose surfaces are coated to provide high reflectivity is called Fabry-Perot etalon. Incident beam is multiply reflected: the amplitudes of multiply reflected beams decrease geometrically. Essentially an infinite number of beams participate in interference both in reflection and in transmission. The irradiance distribution in transmission of a Fabry-Perot etalon is given by

$$I(\delta) = I_0 \frac{1}{1 + F\sin^2(\delta/2)} : \quad \delta = \frac{2\pi}{\lambda} 2nt\cos\theta_t = 2m\pi$$

where θ_t is the angle of refraction inside the plate, m is the fringe order and the parameter F is defined as $F = 4R/(1-R)^2$: R is the reflectivity of the surfaces. This distribution is also called Airy distribution. Another parameter of interest is the finesse $\mathcal{F}$, which determines the resolving power of the interferometer. It is defined as

$$\mathcal{F} = \frac{\textit{Fringe separation}}{\textit{Full Width Half Height}} = \frac{2\pi}{4}\sqrt{F} = \frac{\pi}{2}\sqrt{F}$$

The formula for full width at half height (FWHH) given in the books is

$$FWHH = 4/\sqrt{F}$$

This assumes that the minimum of irradiance distribution is zero. As is evident from Fig 4, the minimum irradiance is zero only for cases where reflectivity of the surfaces is very high. A correct formula that represents correct FWHH for all reflectivity values is

$$FWHH = 4/\sqrt{F+2}$$

It is seen that phase difference between successive transmitted beams depends on θ_t and hence the fringes are fringes of constant inclination and are circular.

Figure 4 is the irradiance distribution in the fringe pattern of a Fabry-Perot interferometer. Sharpening of the fringes can be seen as the reflectivity of the surfaces increases.

Prior to Fabry-Perot interferometer or etalon, multiple beams were created by employing high reflectivity of a surface at larger angles of incidence such as in Lummer-Gehrcke plate. Because of oblique incidence and finite length of the plate, only finite number of beams participates in interference. However, multiple beam interference in both transmission and reflection could be simultaneously seen or recorded. The irradiance distribution, both in reflection and transmission (when the first reflected beam is blocked) is of the type

$$I(\delta) = I_0 \frac{1 + F_N\sin^2(N\delta/2)}{1 + F\sin^2(\delta/2)}$$

where $F_N = 4R^N/(1-R^N)^2$ and N is the number of beams. The phase difference δ is given by $\delta = \frac{2\pi}{\lambda} 2nt\cos\theta_t$. The expression for phase difference is same as that for F-P etalon but the angle θ_t is much larger compared to that in F-P etalon. Phase difference between successive beams in multiple-beam interferometry with amplitude division is constant and hence all the beams meet in phase for constructive interference.

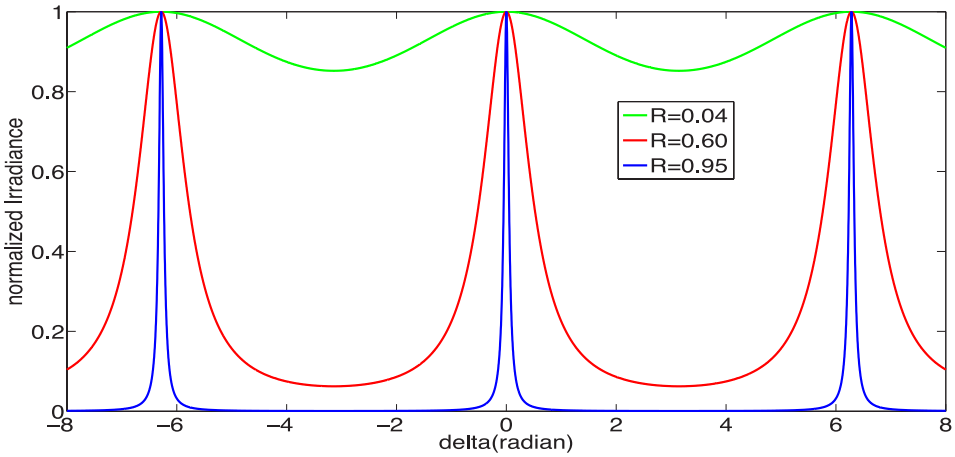

Fig 4. Irradiance distribution for several values of reflectivity

Table 1 gives comparison of some parameters.

Table 1. Some Relevant Parameters

Types		FWHH	$\mathcal{F}$	$\mathcal{R}$	$\Delta\lambda_{fsr}$
Two beam		π	2	–	–
Multiple beam	Grating	$2\pi/N$	N	mN	λ/m
	F-P interferometer	$4/\sqrt{F+2}$	$\pi\sqrt{F+2}/2$	m$\mathcal{F}$	λ^2/2t: θ_t=0
	F-P etalon	$4/\sqrt{F+2}$	$\pi\sqrt{F+2}/2$	m$\mathcal{F}$	λ^2/2nt: θ_t=0
	L-G Plate	$4/\sqrt{F-2N^2F_N}$	$\pi/\sqrt{F-2N^2F_N/2}$	m$\mathcal{F}$	λ^2/2nt cosθ_t

Multiple beam interferometers described above are high-resolution systems used for spectroscopy.

Fizeau multiple-beam interferometer

Only application of multiple-beam interferometry for testing, particularly surface evaluation, is by Fizeau interferometer. Its distinctive features are that the surfaces are very close to each other and they enclose a small angle. It is essentially multiple beam interference in a very thin air wedge. Due to a small angle between the reflecting surfaces there is increasing phase difference between the successive beams and spatial walk-off the beam. This results in interference of finite number of beams with increasing phase difference and the fringes are localized in the wedge. As a consequence the irradiance distribution departs from the Airy distribution showing asymmetry and undulations. Since the fringes are very sharp, surface information is available on and near the fringes, some sort of scanning needs to be done to scan the whole surface. Following Brossel, the phase difference for the p^{th} beam can be written as [16]

$$\delta_p = \frac{2\pi}{\lambda}\left(2p\alpha y - \frac{4}{3}p^3\alpha^2 y\right)$$

In order that the p^{th} beam does not interfere destructively with the first beam, the excess path should be less than $\lambda/2$, i.e.,

$$\frac{4}{3} p^3 \alpha^2 y < \frac{\lambda}{2}$$

In fact the phase difference δ_p calculated using Brossel's approach agrees with that obtained using a rigorous approach when p is large [17]. In practice Fizeau multiple-beam interferometry is carried out with very small gap between the two surfaces (low order interferometry) [18]. Roychoudhuri has given a good description of multiple-beam interferometers and their applications [19].

Multiple-beam shear interferometry

Plane parallel plate shear interferometry, first introduced by Murty [20], is an ideal choice to be used as multiple-beam shear interferometry in which both surfaces of the plate are coated. Mallick and Rousseau described multiple-beam lateral shear interferometer in 1973 [21]. In multiple-beam shearing interferometry, an aberrated beam is multiply reflected inside the plate as shown in Fig 5. Beams both in reflection and transmission are sheared: shear can be adjusted by changing the angle of incidence of the aberrated beam.

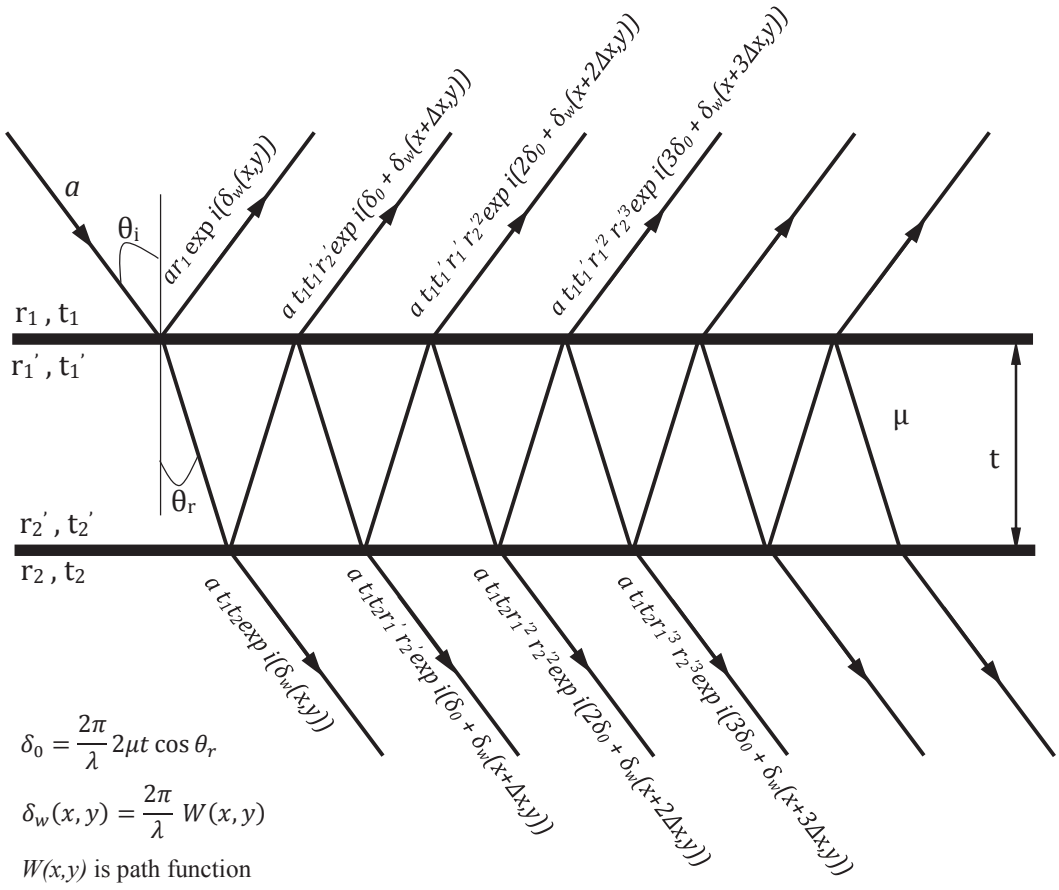

Fig 5. Multiple beams in shear interferometry

The resultant amplitude in reflection A_r is expressed as

$$A_r = a\, e^{i\delta_w(x,y)} [r + tt' r' e^{i\delta'} (1 + r'^2 e^{i\delta'} + r'^4 e^{i2\delta'} + r'^6 e^{i3\delta'} + ...)]$$

where, $\delta' = \delta_0 + \delta_w (x + \Delta x, y) - \delta_w (x,y) = \delta_0 + 2\pi/\lambda\ [W(x + \Delta x,y) - W(x,y)]$ and Δx is the shear along x-direction. The shear Δx is given by

$$\Delta x = 2t \tan\theta_r \cos\theta_i = 2t \cos\theta_i \sin\theta_i (\mu^2 - sin^2\theta_i)^{-1/2}$$

For near normal incidence, the shear is $2t\theta_i/\mu$.

The infinite series can be summed up to give

$$A_r = a\, e^{i\delta_W(x,y)}\left[r + \frac{tt'r'e^{i\delta'}}{1 - r'^2\, e^{i\delta'}}\right] = a\, e^{i\delta_W(x,y)}\left[\frac{r - (tt' + r'^2)re^{i\delta'}}{1 - r'^2\, e^{i\delta'}}\right] = a\, r\, e^{i\delta_W(x,y)}\frac{1 - e^{i\delta'}}{1 - r'^2\, e^{i\delta'}}$$

The irradiance distribution in the interference pattern in reflection is

$$I_r = A_r A_r^* = I_0 \frac{4R \sin^2\frac{\delta'}{2}}{(1-R)^2 + 4R \sin^2\frac{\delta'}{2}} = I_0 \frac{F \sin^2\frac{\delta'}{2}}{1 + F \sin^2\frac{\delta'}{2}}$$

where parameter F is given by $F = \frac{4R}{(1-R)^2}$. This is exactly what is obtained in the case of Fabry-Perot interferometer. Due to the shear, there will be walk-off of the beam and hence the number of beams participating in interference will be finite.

The bright fringes are formed when

$$\delta' = \delta_0 + \frac{2\pi}{\lambda}\,[W(x + \Delta x, y) - W(x,y)] = (2m + 1)\,\pi : m \text{ is an integer}$$

Since δ_0 is constant, the condition for bright fringes can be expressed as

$$W(x + \Delta x,y) - W(x,y) = \Delta x \frac{\partial W}{\partial x} = (2m + 1)\frac{\lambda}{2}$$

It is assumed that the shear is very small so that the higher derivatives have been ignored. The fringes are loci of x-derivative of the path function. The x-component of the transverse ray aberration d_x is give by

$$d_x = f \frac{\partial W}{\partial x}$$

The y-component is obtained by shearing the wavefront along y- direction, i.e. by rotating the shear-plate by 90º and conducting the experiment.

Transverse ray aberrations can also be obtained in transmission. It is far easy to conduct experiments in transmission when the shear is small and the incidence is near normal. However small shear leads to low sensitivity but almost whole pupil is used.

Coated Wedge shear-plate

If a coated wedge-plate is used as a shear plate with wedge edge along the direction of shear, the fringe formation, in transmission, is governed by

$$\frac{\partial W}{\partial x}\Delta x - 2\mu\alpha y = m'\lambda$$

where α is the wedge angle and y-direction is perpendicular to the wedge edge. The component d_x of the transverse ray aberration is given by

$$d_x = f\frac{\partial W}{\partial x} = \frac{2\mu\alpha y f}{\Delta x} + \frac{m'}{\Delta x}\lambda f$$

Zeroth order ($m' = 0$) fringe gives the locus of the x-component of transverse ray aberration, i.e.,

$$d_x = \frac{2\mu\alpha y f}{\Delta x} \text{ or } y = \frac{\Delta x}{2\mu\alpha f} d_x$$

The locus of the zeroth-order interference fringe therefore maps out the lateral aberration curve with a magnification of $\Delta x/2\mu\alpha f$. Therefore, higher sensitivity is obtained for a smaller value of α; an optimum choice of α must yield one or two fringes in the interferogram. The sensitivity of the method is dependent on the amount of shear, Δx; smaller shear results in lower sensitivity. However, for larger shear the difference between the path functions rather than the gradient should be used in the evaluation of the interferogram.

Sirohi *et al* has employed multiple-beam shear interferometry, both in reflection and transmission, for lens testing [22-24]. Senthilkumaran *et al* has used it for collimation testing [25].

Figure 6 shows a multiple-beam shear interferogram of an on-axis aberrated wave from a lens under test [23].

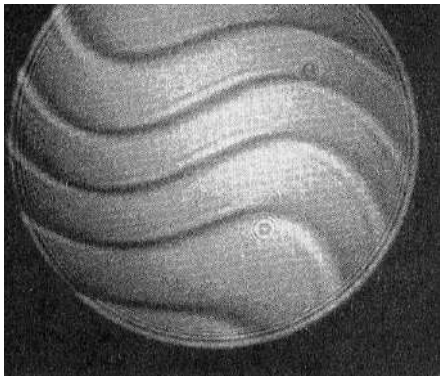

Fig 6. Multiple beam shear interferogram of a lens (from Ref 22)

Multiple-beam wedge plate shear interferometry has been used to measure the focal length of a lens [26]. The wedge plate has a very small angle such that only one fringe is obtained in the interferogram: the fringe is sharp and its inclination can be read accurately.

Multi-wavelength interferometry

Prior to the arrival of laser, all interferometers used quasi-monochromatic light. One application where more than one wavelength was used sequentially was the gage-block interferometer. The length of a gage-block was obtained by measuring fringe fractions at least at three wavelengths provided its length was known within a certain uncertainty. Later the interferometer used three different stabilized lasers: Köster gage block interferometer is an example [27]. Essentially it is a two-beam interferometry with different wavelengths used sequentially.

First two-wavelength interferometer is Hewlett-Packard ac interferometer, which uses Zeeman split two-wavelength He-Ne laser [28]. The two wavelengths are separated: optical wave of one wavelength acts as a reference to the other creating a beat signal. The beat frequency changes during measurement. This interferometer is the workhorse of machine tool industry.

In heterodyne interferometry, a small frequency shift is introduced in one arm of the interferometer with a pair of AO modulators [29]. The output current from the photo-detector is proportional to

$$i(x,y;t) \propto a_{01}^2 + a_{02}^2 + 2a_{01}a_{02}\cos[2\pi(\nu_1 - \nu_2)t - \Delta\phi(x,y)]$$

where a_{01} and a_{02} are the amplitudes of two waves with frequencies ν_1 and ν_2 and their phases $\phi_1(x,y)$ and $\phi_2(x,y)$, respectively: $\Delta\phi(x,y) = \phi_1(x,y) - \phi_2(x,y)$.The output from a photo-detector at this point is modulated at a frequency $(\nu_1 - \nu_2)$, and the phase of this modulation corresponds to the original phase difference between the interfering waves. The phase of the modulation can be measured electronically with respect to a reference signal derived either from a second detector to which the optical paths remain unchanged, or from the source

driving the modulator. This technique is capable of very high precision and has been used for a variety of measurements [30].

The wavelength of a laser diode can be varied by changing the injection current. If the optical path difference between the arms of an interferometer is d and the frequency of the diode laser is varied linearly by linearly ramping the injection current, then the frequency of the beat signal f is given by

$$f = \frac{dm}{dt} = \frac{d}{c}\frac{dv}{dt} \rightarrow\rightarrow d = (f\,c)/\frac{dv}{dt}$$

where ν is the frequency of light wave and c is the velocity of light. The frequency of the beat signal for the fringe count is proportional to the product of the amount by which the frequency of the laser source is shifted and the path difference between the two arms of the interferometer [31].

Synthetic wavelength

Spectral or single wavelength interferometry has very high sensitivity but very small unambiguous range. An optical path difference of Δ gives the same interferometric information as the optical path of (m λ + Δ). Unambiguous range can be increased when two wavelengths λ_1 and λ_2 are used: this gives a synthetic wavelength $\Lambda = \lambda_1\,\lambda_2/(\lambda_1 - \lambda_2)$, which is several times larger than the individual wavelengths. The measurement range now is Λ/2 instead of $\lambda_1/2$ or $\lambda_2/2$. The measurement range is larger when the two wavelengths are closer. Longer paths can be measured by counting fringe order of the synthetic wavelength. The measurement uncertainty is increased if the measured path length *d* is calculated using the synthetic wavelength. Uncertainty in phase measurements is scaled by the ratio of synthetic to optical wavelength. To overcome this problem, more wavelengths can be used, which offer different synthetic wavelengths. Starting from the longest one, each synthetic wavelength is used to get the fringe order of the next shorter one and finally that of an optical wavelength [32].

If a white light source is used in an interferometer the best contrast interference fringes are obtained only when the two paths in the interferometer are equal. If the sample arm of the object is varied, height/depth variations across the sample can be determined by looking at the interferogram at sample positions for which the fringe contrast is maximum. The white light interferogram is used as a setting criterion. Essentially phase ambiguity problem is overcome by using white light. White light interferometry is an important technique not only for surface examination [33] but in other fields as well [34].

3 Conclusion

Interferometry as a measurement technique has benefitted with the advancement of technology. Use of CCD/CMOS devices as detectors, lasers as coherent sources and desktop computing power has enabled it to be a very versatile and precise technique. Automatic evaluation of interferograms and presentation of results that could be understood by unskilled persons is a common feature in all commercial interferometers used either for displacement measurement, or for optical and surface testing, or for profiling of the objects.

References

1. Born M, Wolf E, Principles of Optics, 4th edn, (Pergamon Press), 1970.
2. Candler C, Modern Interferometers, (Hilger and Watts, London), 1951.
3. Steel W H, Interferometry, (Cambridge University Press, Cambridge, UK), 1983.
4. Hariharan P, Optical Interferometry, (Academic Press), 2003.
5. Langenbeck P, Multipass Twyman–Green Interferometer, *Appl Opt*, 6(1967)1425-1426.
6. Langenbeck P, Multipass Interferometry, *Appl Opt*, 8(1969)545-552.
7. Bubis I Y, Multipass Interferometer for Surface Shape Inspection, *Sov J Opt Technol*, 39(1972)411-413.

8. Gerchman M C, Hunter G C, Differential Technique for Accurately Measuring the Radius of Curvature of Long Radius Concave Optical Surfaces, *Proc SPIE*, 192(1979)75-84.
9. Hariharan P, Sen D, Double-Passed Two-Beam Interferometers, *J Opt Soc Am*, 50(1960)357-361.
10. Zhang Tiejun, Yonemura Motoki, Multipass Michelson interferometer with the use of a wavelength-modulated laser diode, *Appl Opt*, 35(1996)5650-5656.
11. Pisani M, Multiple reflection Michelson interferometer with picometer resolution, *Opt Exp*, 16(2008)21558-21563.
12. Kumar V C P, Joenathan C, Ganesan A, Somasundram U, Increasing the sensitivity for tilt measurement using a cyclic interferometer with multiple reflections, *Opt Eng*, 55(2016)084103; doi.org/10.1117/1.OE.55.8.084103
13. Joenathan C, Naderishahab T, Bernal A, KrovetzA B, Pretheesh Kumar V C, Ganesan A R., Nanoscale tilt measurement using a cyclic interferometer with polarization phase stepping and multiple reflections, *Appl Opt*, 57(2018)B52-B58.
14. Joenathan C, Bernal A, Woonghee Y, Bunch R M, Hakodac C, Dual-arm multiple-reflection Michelson interferometer for large multiple reflections and increased sensitivity, *Opt Eng*, 55(2016) 024101; doi. org/10.1117/1.OE.55.2.024101
15. Vikram C S, Sirohi R S, Use of phase holograms for phase difference amplification, *Opt Commun*, 2(1971)444-446.
16. Brossel J, Multiple-beam localized fringes: part I. - Intensity distribution and localization, *Proc Phys Soc*, 59(1947) 224-234.
17. Born M, Wolf E, *Principles of Optics*, fourth edition, (Pergamon Press), 1970, pp 351-358.
18. Tolansky S, Multiple-Beam Interferometry of Surfaces and Films, (Oxford University Press, Oxford, (1948), Dover, New York), 1970.
19. Roychoudhuri C, Multiple-Beam Interferometers, in *Optical Shop Testing*, (Ed) Malacara D, (John Wiley & Sons, Inc., Hoboken, New Jersey), 2007.
20. Murty M V R K, The Use of a Single Plane Parallel Plate as a Lateral Shearing Interferometer with a Visible Gas Laser Source, *Appl Opt*, 3(1964)531-534.
21. Mallick S, Rousseau M, Multiple-Beam Lateral-Shear Interferometer, *Appl Opt*, 12(1973)2305-2308.
22. Sirohi R S, Eiju T, Matsuda K, Barnes T H, Multiple-beam lateral shear interferometry for optical testing, *Appl Opt*, 34(1995)2864-2870.
23. Sirohi Rajpal S, Eiju Tomaoki, Matsuda Kiyofumi, Barnes Thomas H, Reflection Multiple beam wedge plate shear interferometry for lens testing, *Opt Rev*, 1(1994)293-295.
24. Sirohi R S, Eiju T K, Matsuda, Senthilkumaran P, Multiple beam wedge plate shear interferometry in transmission, *J Mod Opt*, 41(1994)1747-1755.
25. Senthilkumaran P, Sriram K V, Kothiyal M P, Sirohi R S, Multiple beam wedge plate shear interferometer for collimation testing, *Appl Opt*, 34(1955)1197-1202.
26. Matsuda Kiyofumi, Barnes Thomas H, Oreb Bob F, Sheppard Colin J R, Focal-length measurement by multiple-beam shearing interferometry, *Appl Opt*, 38(1999)3542-3548.
27. Decker J E, Schödel R, Bönsch G, Next-Generation Kösters Interferometer, *Proceedings of SPIE*, 5190(2003) 14-23.
28. Christopher Burns, Deane A Gardner, Robert C Quenelle, Lawrence J Wuerz, A New Microcomputer-Controlled Laser Dimensional Measurement and Analysis System, *Hewlett-Packard Journal*, 34(1983)3-13.
29. Lavan Michael, Cadwallender W K, Deyoung T F, Heterodyne interferometer to determine relative optical phase changes, Review of Scientific Instruments, 46(1975)525-527.
30. Ohtsuka Y, Sasaki I, Laser heterodyne measurement of small arbitrary displacements, *Opt Commun*, 10(1974) 362-365.
31. Stone J A, Stejskal A, Howard L, Absolute interferometry with a 670-nm external cavity diode laser, *Appl Opt*, 38(1999)5981-5994.
32. Dändliker R, Hug K, Zimmermann E, Schnell U, Multiple Wavelength and White-Light Interferometry, 2nd Japan-France Congress on Mechatronics, Nov 1-3, Takamatsu, Japan, (1994)

33. de Groot P, Deck L, Surface profiling by analysis of white-light interferograms in the spatial frequency domain, *J Modern Optics*, 42(1995)389-401.

34. Mehta D S, Srivastava V, White Light Phase-Shifting Interference Microscopy for Quantitative Phase Imaging of Red Blood Cells, Fringe 2013 – 7th International Workshop on Advanced Imaging and Metrology, 581-584, Wolfgang Osten (ed), Springer, Verlag Heidelberg, 2014.

[Received: 14.12.2019]